A CFD-based Study on the Effect of Cone Height of an Elevated Rotor on the Performance of Radial Blowers

ESRA H. ISIK[1], MUSTAFA SENGUL[2] and I. BEDII OZDEMIR[3]
Fluids Group
Istanbul Technical University
Faculty of Mechanical Engineering
Gumussuyu 34437 ISTANBUL
TURKEY
[1,2]Research student, [3]Professor, bozdemir@itu.edu.tr http://www.akis.itu.edu.tr

Abstract: - In this paper, a family of six radial blowers with differently elevated rotor cones have been studied to examine the effect of the cone height on the blower performance. In the design process of the blower family, the airfoil type impellers were used (NACA 25010), and all other parameters; the inlet-outlet port angles, the number of impellers and the rotor-base diameter were kept constant. The blowers were run with a rotational speed of 9,000 rpm and exposed to the pressure loads from 3,000 to 12,000 Pa. Results show that increasing the ratio of the rotor cone-height to the cone-base diameter certainly has a future prospect to develop the performance of the radial blowers. In that, the blowers with elevated cones can withstand to very large pressure loads, which were unreachable by the flat blowers. However, it seems that beyond an optimum ratio, which appeared to be 0.378 in this investigation, the performance seems to drop.

Key-Words: - Centrifugal fans, Computational fluid dynamics, Elevated conical rotor.

1 Introduction

Radial blowers have been used in a wide range of engineering applications as, for example, in heating and cooling industry, blowing, aeration and drying processes, vacuum lifting, vacuum cleaning and pneumatic transportation in textile and cement industries [1-3]. In these machines, the air enters through an inlet section in the direction of rotor axis and turns by 90 degrees to the radial direction. The flow is accelerated by the rotating blades positioned on a disc type rotor. Flow exiting the rotor is collected by a casing, which is variously called as a squirrel or stator in which the pressure of fluid increases as the velocity gradually decreases from the tongue to the outlet section. Finally, the air is delivered to the downstream ducting or pipe for final use [4].

It is obvious that the design parameters of radial blowers are needed to be determined according to its intended use. Like any air moving machine, the basic design parameters of the blowers, which are affecting the efficiency and power ratings of the machine are known to be the flow rate, pressure rise (or load) and rpm of the machine as well as the design of the ports etc. Yet, the legislative regulations [5] have today become tighter with concerns on sustainability and impacts on the environment and climate change. In particular, reducing the carbon footprints of processes, increased demand for low-noise, energy-efficient and compact machines. These are the constraints added on top of commercial viability issues, which still necessitate low-cost production [6]. Furthermore, these requirements are mostly contradicting, and this has led the designers to explore other relatively less explored parameters. In recent years [7], the positioning of impellers on an elevated conical-base (rather than disc-like base) rotors has been proven to increase the performance of the radial blowers to the limits which were previously inconceivable. Therefore, it became crucially important to investigate the performance bounds of a family of radial blowers, with different cone aspect ratios, AR (ratio of the cone height, H to the cone base diameter, D). However, creation a family of radial blowers having the same impeller form is a challenging problem, entailing very special design conception, procedures and, of course, programing tools.

In the vast majority of literature up to now, the radial blower optimizations and numerical solutions seemed to have an emphasis on parameters like the blade type, inlet and outlet angles, number of impellers and impeller height and thickness [8]. It has been known that increasing the number of impellers and the impeller height of a blower with constant thickness increases the flow rate and the pressure rise. Yet again, if the impeller height is

increased and the diameter is kept the same, the flow rate seems to increase [2]. Contrarily, keeping the impeller height constant, but increasing the rotor diameter decreases the flow rate. It has been evidenced that improvements in the efficiency and total working pressure with an increase in the impeller height can continue up to an optimal point beyond which they all decline [9]. Furthermore, it has been known that increasing the outlet angle while keeping the all conditions constant, degrades the efficiency [10]. In general, the airfoil type blades have shown superior performance compared to the blades with constant thickness [11].

It appears that the effect of aspect ratio on the blower performance was not fully investigated for a family of blowers with the same number of blades, blade type, inlet-outlet angles and rotor base diameter. In this study, the relationship between the cone height (so the aspect ratio) of a radial blower and the performance parameters like, the flow rate and the pressure rise has been studied by exploiting a powerful in-house numerical blower design tool [12] and the computational fluid dynamics (CFD) so that expensive prototyping and experimentation were avoided.

2 Numerical Blower Design Procedures

The approach briefly described here is based on the procedures described in [13] and aiming at designing compact high speed, high pressure radial blowers. It is known that radial machines with improperly designed blade geometry often suffer from poor flow conditions, leading to turbulent fluctuations and separation over the impeller walls. These constitute the main sources of the aero-acoustic noise and generally produce broadband gust signals. In some cases, they, however, trigger selectively organized structures over the impeller surfaces causing tonal self-noise. Furthermore, the spectral characteristics of the noise may also change along the impeller cascade from the inlet to the outlet of the rotor.

The proper designs to reduce these artifacts depend on the accurate calculations of lift and drag forces using the mass and momentum balances on flow passages surrounding a generic airfoil. The forces can be exploited to improve the shape parameters (camber, chord length and thickness) and the local angle of attack of airfoils in an iterative procedure, which results in correct pressure head and flow rate for a given rpm and geometry (rotor base diameter and height) [13]. This approach requires a look-up table for the airfoil shapes versus lift coefficient. It is also important to consider the losses associated with turbulence and cross-flow effects along the blades. Once the rotor is designed, the flow from each cascade is used to design the squirrel in a second iterative process; the mass and momentum balances together with the turbulent losses are included to calculate the polar profile of the squirrel. The main concern here is to keep the static pressure constant, so that the rotor is not exposed to non-uniform pressure forces. The algorithm described above is developed and programmed in an in-house code called PRD [13]. The outputs of the code are the point clouds describing surfaces of the rotor and squirrel, and a text file tabulating some critical data as, for example, the number of impellers, solidity etc.

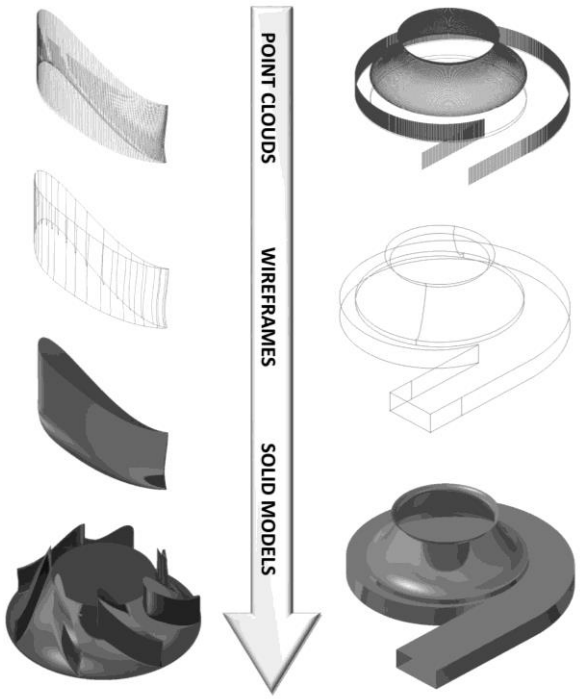

Fig. 1. Schematic of the design process from point cloud to solid model.

Fig. 1 illustrates how the solid geometries of the rotor and the squirrel were obtained from the point clouds. The code also allows defining the radial velocity profile at the pressure side of the rotor so that the radial velocity diminishes near the rotor base and at the tip, which suppress the tip vortices and, so the tip noise.

In the present study, by keeping the rotation of the blowers at 9000 rpm and the rotor diameter D 132.3 mm, a family of six radial blowers was designed with changing the cone height, H as 0, 10, 30, 50, 70 and 90 mm. The aspect ratio of the corresponding blower designs (B1 - B6) were tabulated in Table 1. Figs. 2 and 3 show the design

features of the resulting rotors and squirrels, respectively.

Table 1. Aspect ratios of the blowers.

Blower code	Height (*H*) [mm]	AR (*H/D*)
B1	0	0
B2	10	0.076
B3	30	0.227
B4	50	0.378
B5	70	0.529
B6	90	0.680

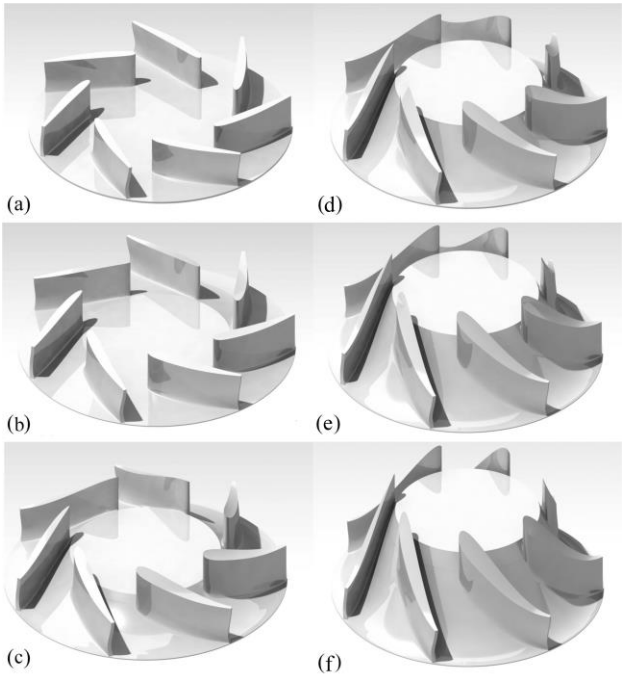

Fig. 2. Rotors with different aspect ratios, (a) B1, (b) B2, (c) B3, (d) B4, (e) B5 and (f) B6.

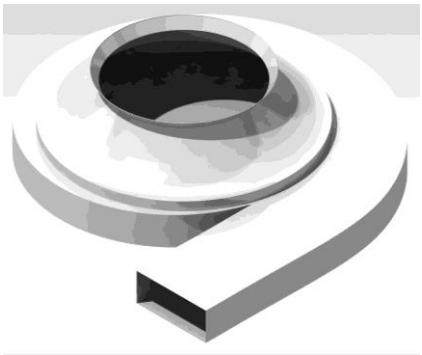

Fig. 3. A typical squirrel.

3 Governing Equations and Computational Procedures

The flow is described by the spatially-averaged Navier-Stokes equations [14]. With the maximum pressure head, the relation derived from the isentropic flow equation [15],

$$\frac{\Delta\rho}{\rho} = \left[1 + \frac{\Delta p}{p}\right]^{1/\gamma} - 1 \quad (1)$$

(where γ is being the specific heat ratios) gives a relative density change of 2.1% and, therefore, the flow was accepted as incompressible. Hence, using the Cartesian tensor notation, the mass conservation of the fluid is given as,

$$\frac{\partial u_i}{\partial x_i} = 0 \quad (2)$$

where u_i denotes the conventional average of the velocity tensor and ρ density.

The transport equations for the momentum can be expressed as,

$$\rho\frac{\partial u_i}{\partial t} + \rho\frac{\partial (u_i u_j)}{\partial x_j} = \frac{\partial p}{\partial x_j} + \frac{\partial}{\partial x_j}\left\{\mu\left(\frac{\partial u_i}{\partial x_j} + \frac{\partial u_j}{\partial x_i}\right)\right\} \quad (3)$$

where μ is the dynamic viscosity, p is the average pressure and $u_i u_j$ is a term which can be described as Reynolds stress tensor.

The multiple frame of reference (MFR) application [16,17] is able to translate and rotate cell zones at different speeds in order to simulate rotating system. The computational grids of the MFR model consist of two domains, namely the rotary and the stationary domains. This method has been generally used in compressors, fans and blowers. The stationary fluid velocities can be transformed to the rotating frame velocities as [18],

$$\boldsymbol{u}_r = \boldsymbol{u} - \boldsymbol{v}_r \quad (4)$$

$$\boldsymbol{v}_r = \boldsymbol{\omega} \times \boldsymbol{r} \quad (5)$$

where $\boldsymbol{u}_r$ is the velocity vector relative to the rotating frame zone and $\boldsymbol{u}$ is the absolute velocity vector. Moreover, $\boldsymbol{\omega}$ is the angular velocity vector and $\boldsymbol{r}$ is the position vector of the rotating frame. Hence,

$$\nabla \cdot \boldsymbol{u}_r = 0 \quad (6)$$

$$\frac{\partial}{\partial t}\rho\boldsymbol{u} + \nabla\cdot(\rho\boldsymbol{u}_r\boldsymbol{u}) + \rho(\boldsymbol{\omega}\times\boldsymbol{u}) = -\nabla p + \nabla\bar{\bar{\tau}} + \boldsymbol{F} \quad (7)$$

where $\bar{\bar{\tau}}$ is the viscous stress defined as,

$$\tau_{ji} = \mu\left(\partial u_j/\partial x_i + \partial u_i/\partial x_j\right) - \frac{2}{3}\mu\,\partial u_l/\partial x_l \delta_{ji}$$

and $(\boldsymbol{\omega} \times \boldsymbol{u})$ is the Coriolis force.

In addition to the equations that the RANS formulation requires, the closure of the turbulent parameters necessitates solving the transport equations for the turbulent kinetic energy (k) equation [19],

$$\frac{\partial(\rho k)}{\partial t} + \frac{\partial(\rho k u_i)}{\partial x_i} = \frac{\partial}{\partial x_i}\left[\left(\mu + \frac{\mu_t}{\sigma_k}\right)\frac{\partial k}{\partial x_i}\right] + P_k + P_b - \rho\varepsilon - Y_M + S_k \quad (8)$$

and the equation for rate of dissipation (ε),

$$\frac{\partial(\rho\varepsilon)}{\partial t} + \frac{\partial(\rho\varepsilon u_i)}{\partial x_i} = \frac{\partial}{\partial x_i}\left[\left(\mu + \frac{\mu_t}{\sigma_\varepsilon}\right)\frac{\partial \varepsilon}{\partial x_i}\right] - \rho C_1 S_\varepsilon - \rho C_2 \frac{\varepsilon^2}{k+\sqrt{\nu\varepsilon}} + C_{1\varepsilon}\frac{\varepsilon}{k} C_{3\varepsilon} P_b + S_\varepsilon \quad (9)$$

In these equations P_k is the generation of turbulence kinetic energy, which stems from the mean velocity gradients and P_b represents the generation of turbulence kinetic energy due to buoyancy. S_k and S_ε are the source terms. Finally, the turbulent viscosity is defined as,

$$\mu_t = \rho C_\mu \frac{k^2}{\varepsilon} \quad (10)$$

The coefficients σ_k, σ_ε, $C_{1\varepsilon}$, $C_{2\varepsilon}$ are the standard constants [14]. In the present simulations, realizable k-ε turbulence model, which demonstrates a superior ability to capture the average flow of complex structures in flows with rotation, separation and circulation [20, 21], was preferred to the standard k-ε turbulence model [19].

The computations were performed by using the finite volume method, which works for structured, as well as for unstructured meshes. Therefore, it is more suitable for flows in complex geometries [22]. In order to avoid sharp changes in the streamline curvature at the entrance of the rotor, the inlet boundary was located on a semi-spherical surface attached to the inlet diffuser, which also ensured a fully-developed flow prevailed at the rotor entrance. At the inflow, a first-type (Dirichlet) boundary condition [14,23] was used for the pressure with a prescribed value of zero Pa and the velocities were set perpendicular to the semi-spherical surface (Fig. 4). Except for the intersection surfaces of the rotor and squirrel, named as the interface, all other surfaces are defined as wall with no-slip.

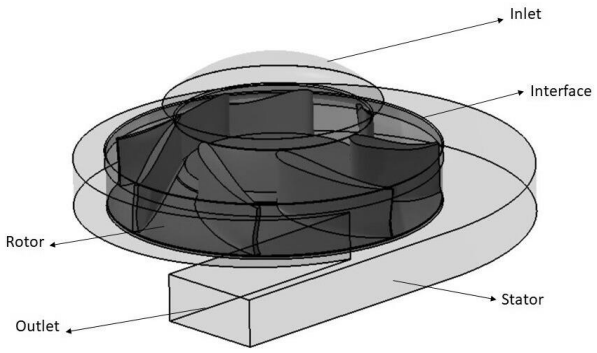

Fig. 4 Schematic for the descriptions of the boundary conditions.

At the outlet, four different prescribed pressures; 500 Pa, 3000 Pa, 10,000 Pa and 12,000 Pa were used to build the performance curves of the different blowers. A second-type (Neumann) boundary condition was applied for velocities at the outflow boundaries. In order to minimize the influence of outflow boundary, the length of the computational domain was extended in the outlet direction up to two wetted diameters of the squirrel exit. Besides, very steep velocity gradients were anticipated at the rotor entrance and rotor-squirrel interface and, therefore, the mesh resolutions in these regions were very important [24]: An improper resolution could either degrade the accuracy of the calculations or excessively increase the computational effort. Keeping this in mind, first, a mesh independence study was performed for the blower with AR = 0.227 at 3000 Pa pressure rise and 9000 rpm. The effect of the mesh size (from course to fine mesh) on the volumetric flow rate is presented in Table 2, where the mesh size of 4.5×10^6 seems adequate for accurate results. Hence, as a compromise, the solution domain in the present case was discretized into 4.5 million cells (Fig. 5), which also assured an adequate resolution in the critical regions.

Table 2 Mesh check results.

Mesh Size	Flow Rate [m^3/s]
2.1×10^6	0.3112
3.3×10^6	0.3114
4.5×10^6	0.3113
6.0×10^6	0.3113

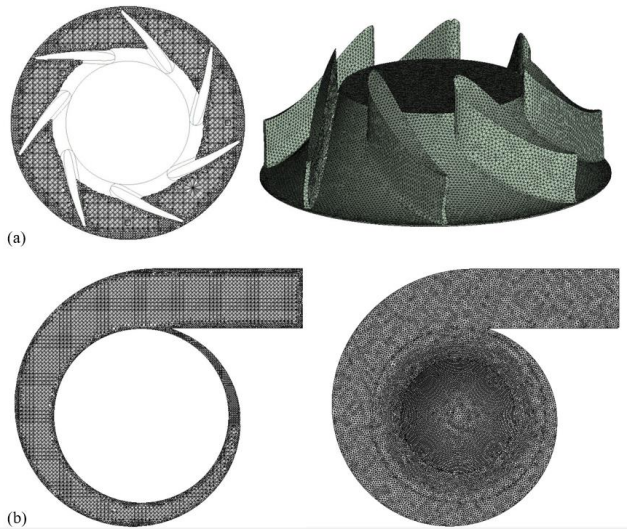

Fig. 5 Examples of; (a) mesh for the rotor and (b) mesh for the squirrel.

Since the solver had the co-located variable arrangement, which requires excessive interpolations, a central differencing scheme [14] was used for the spatial discretization, which preserves a second-order accuracy. The transport equations were solved using the finite-volume method and a commercial software [18], which was parallelized by domain decomposition using the MPI routines. The calculations were performed in a parallel environment with 12 processors. A residual level of 10^{-6} was used in the numerical setup, which was sufficiently accurate for the variables calculated.

4 Results and Discussion

Table 3 shows the performance data obtained from the six simulations with different pressure heads for each blower. It is clear that not all blowers can operate under the given pressure load at the exit. For example, the flat blower B1 (with AR = 0) cannot withstand the pressure loads for 10,000 and 12,000 Pa; the same is also true for the blowers B5 and B6 for the pressure load of 12,000 Pa. The blowers B2, B3 and B4 are able to set a flow at all pressure loads, although the blower B3 mostly performs better than the other two. These results also show that there is an optimum aspect ratio, up to which, an increase in performance can be achieved. The performance starts to degrade by elevating the cone height beyond this point.

Fig. 6 shows the performance curves for all blowers. It is apparent that while the blower B3 exhibits the best performance, the flat blower B1 does by far the worst. If we address the poor performances following the B1 blower, the blowers

Table 3. Volumetric flow rates, Q [m^3/s]

Δp [Pa]	B1	B2	B3	B4	B5	B6
500	0.273	0.339	0.344	0.342	0.335	0.335
3,000	0.214	0.306	0.311	0.308	0.298	0.297
10,000	-	0.176	0.166	0.156	0.113	0.144
12,000	-	0.057	0.002	0.020	-	-

B5 and B6, which have the rotor elevations stretched beyond the optimal point, are also suffering severely. One can easily envisage that the performance degradation at high aspect ratios (B5 and B6) stems from the stalling impellers [25], in which swift changes in the flow direction occur. Severe stall conditions eventually lead to the separation of the flow from the impeller surfaces, resulting in flow reversals in the impeller cascades. It is such vortices, which induce pressure pulses in the flow and reduce the rotor performance. The deprivation of the flow inside the rotor has been observed, especially in high-speed radial blowers and it can be avoided by adding a partial slot at the end of impeller cascades, which saves flow energy [26]. As a typical example of the flow separation is displayed in Fig. 7 for the blower B5 at 12,000 Pa.

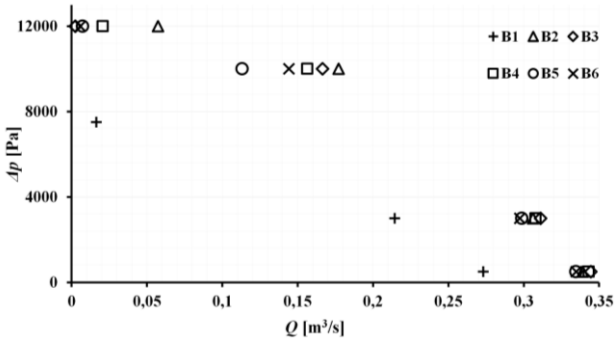

Fig. 6. Blower performance data.

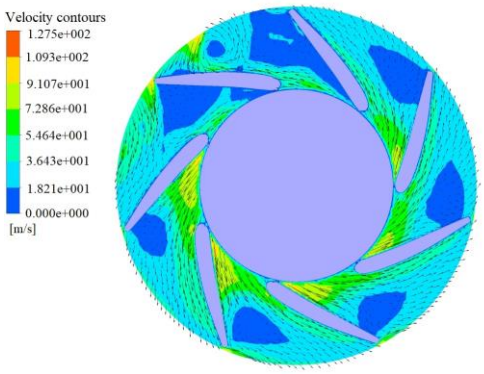

Fig. 7. Flow separation of blower B5 at 12,000 Pa.

It is a usual problem in the radial blowers that the flow includes a secondary motion at the squirrel

exit. This leads to low-frequency turbulent fluctuations, which develops due to inappropriate rotor, squirrel and tongue geometries. As a result, the fluid discharged from the impeller cascades cannot be collected homogeneously by the squirrel and, consequently, a strong swirl develops, forming a large secondary motion in the squirrel. It is apparent in the streamlines plotted in Fig. 8 that almost no swirl exists in the exit section of the squirrel. This is expected because in our blower design algorithm [13] the cross-section of the squirrel is gradually enlarged to satisfy the continuity and to keep the wall static pressure constant along the flow pathway from the tongue to the squirrel exit.

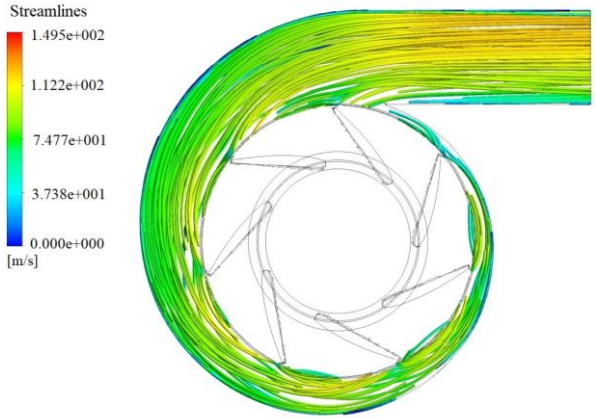

Fig. 8. A typical example of streamlines in the squirrel.

In order to check if the latter design constraint is violated or not, the static pressure data were examined at 10 points on the squirrel back wall (see Fig. 9) from a point downstream of the tongue to the exit section of the squirrel. The values were presented in Fig. 10 for the six blowers, all working at 3,000 Pa. They show very small deviations and this is consistent with the design constraint. It also reaffirms that the blowers B3 and B4 present larger pressure levels in the squirrel compared to the others.

The static pressure contours for a pressure load of 3,000 Pa are presented for all blowers in Fig.11, where the blower B3 has highest maximum pressure compared to the other blowers. It should also be emphasized that at the exit section of the squirrel, all the blowers achieve a uniform pressure distribution.

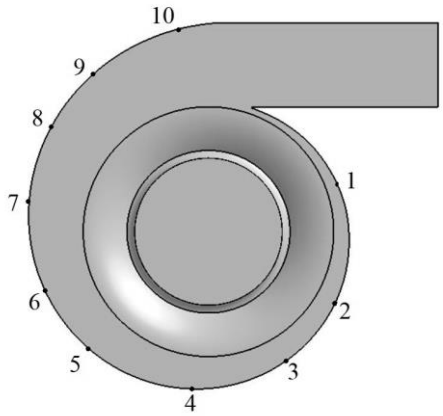

Fig. 9. Sampling locations on the squirrel back wall.

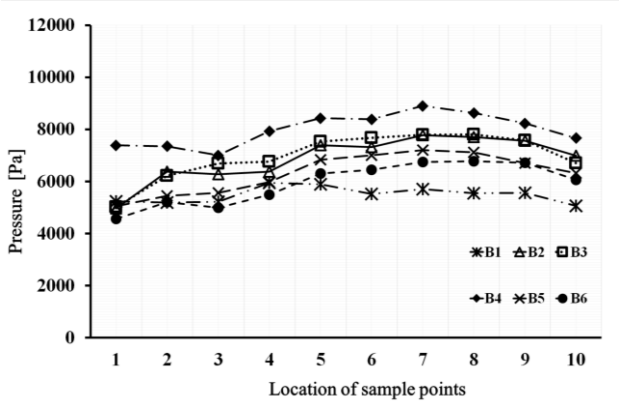

Fig. 10. Pressure variation in the squirrel (see Fig 9 also).

The corresponding velocity contours are presented in Fig. 12. It seems that the highest velocities occur on the squirrel side of the rotor-squirrel interface, but they quickly smeared as the flow from the rotor cascade penetrates deep into the squirrel flow.

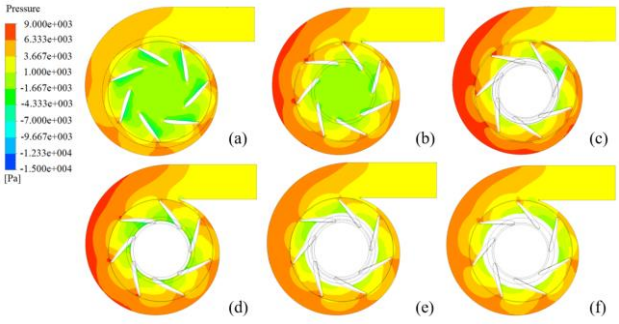

Fig. 11. Pressure contours at a cut-plane of z = 0.04 mm from the bottom (a) B1, (b) B2, (c) B3, (d) B4, (e) B5 and (f) B6.

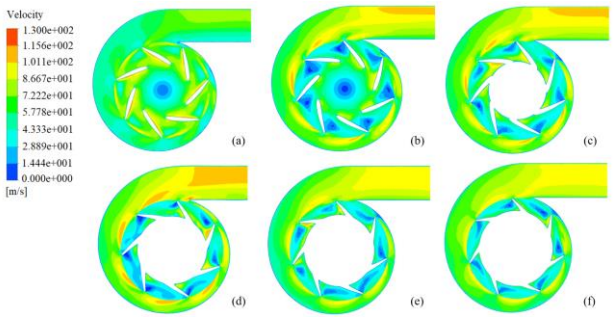

Fig. 12. Velocity contours at a cut-plane of z = 0.04 mm from the bottom (a) B1, (b) B2, (c) B3, (d) B4, (e) B5 and (f) B6.

5 Conclusion

The effect of cone height on the blower performance was investigated using numerical experiments. The conclusions of this study can be summarized as follows;

1. It can be concluded that increasing the elevation of the rotor cone certainly opens a new horizon to improve the performance of the radial blowers. When the aspect ratio is increased, the flow rate of a radial blower can increase about 1.4 times compared to the flat blower. The blowers with elevated cones can also operate under high load values (10,000 Pa - 12,000 Pa) where the flat blower cannot reach.
2. Although increasing the cone height has a positive impact on the performance, the flow rate and the maximum pressure load of the blower decrease beyond an optimum aspect ratio, which was about 0.378 in this study.
3. The squirrel design seems to be critically important to achieve swirl-free flow at the exit of the squirrel and to keep the wall static pressure constant in the squirrel flow. The design algorithm used in this study assures a homogeneous collection of the rotor fluid and precludes the formation of a swirl in the squirrel.

References:

[1] Prezelj, J., & Novakıvic T., Centrifugal fan with inclined blades for vacuum cleaner motor, *Applied Acoustics*, Vol.140, 2018, pp. 13–23.

[2] Galloni, E., Parisi, P., Marignetti, F. & Volpe, G., CFD analyses of radial fan for electric motor cooling, *Thermal Science and Engineering Process*, Vol.8, 2018, pp. 470-476.

[3] Jeon, H.W., Beak, J.S. & Kim, J.C., Analysis of the aeroacoustics characteristics of centrifugal fan in vacuum cleaner, *Journal of Sound and Vibration*, Vol.268, No.5, 2003, pp. 1025-1035.

[4] Song, H., *Engineering Fluid Mechanics*, Springer, 2018.

[5] Energy Efficiency Opportunities Act 2006, www.legislation.gov.au. Retrieved 2019-11-25.

[6] Dawes, W.N., Dhanasekaran, P.C., Demargne, A.A.J., Kellar, W.P. & Savill, A.M., Reducing bottlenecks in the CAD-to-Mesh-to-Solution cycle time to allow CFD to participate in design, *Journal of Turbomachinery*, Vol.123, No.3, 2001, pp. 552-557.

[7] Culjat, M., Singh, R. & Lee, H. Mechanical circulatory devices in *Medical Devices: Surgical and Image-Guided Technologies*, John Wiley & Sons, pp 240-241, 2012.

[8] Singh, O.P, Khilwani, R., Sreenivasulu, T. & Kannan, M., Parametric study of centrifugal fan performance: Experiments and numerical simulation, *International Journal of Advances in Engineerring & Technology*, Vol.1, 2011, pp. 33–50.

[9] Huang, K.C. & Hsieh E.M., Performance analysis and optimized design of backward-curved airfoil centrifugal blowers, *HVAC&R RESEARC*, Vol.15, 2009, pp. 461-488.

[10] Zhang, L., Wang, L.S., Wu, F.D. & Zhang, Q., Numerical study for centrifugal fan based on parametric method, *Applied Mechanics and Materials*, Vol.55-57, 2011, pp. 892-897.

[11] Patel, K.K., Performance analysis and optimization of centrifugal fan, *International Journal of Emerging Trends in Engineering and Development*, Vol.2, 2013, pp. 261-270.

[12] Ozdemir, I.B. A design tool for radial flow machines, Fluids Group Report FGR-2006-8, 2006.

[13] Ozdemir, I.B. New design concepts in radial blowers, http://www.akis.itu.edu.tr/research/High_Performance_Radial_Fan.pdf. Retrieved 2019-11-25.

[14] Ferziger, J.H. & Peric, M., *Computational Methods for Fluid Dynamics*, Springer, 2002.

[15] Shapiro, A.H. *The Dynamics and Thermodynamics of Compressible Fluid Flow*; Volume 1, The Roland Press Co., 1954.

[16] Luo, J.Y., Issa, & Gosman A. D. Prediction of impeller-induced flows in mixing vessels using Multiple Frames of Reference. In *IChemE Symposium Series*, number 136, pages 549-556, 1994.

[17] Dogruoz, M.B. & Shankaran, G. Computations with the multiple reference frame technique: Flow and temperature fields downstream of an axial fan, *Numerical Heat Transfer, Part A: Applications*, Vol. 71, 2017, pp. 488-510.
[18] Ansys, *Ansys v17.0 Fluent User's Guide*, USA, 2015.
[19] Blazek, J., *Computational Fluid Dynamics: Principles and Applications*, Elsevier, 2001.
[20] Howard, J.H.G., Patankar, S.V. & Bordynuik, R.M. Flow prediction in rotating ducts using Coriolis-modified turbulence models. *ASME J. Fluids Eng.* Vol. 102, 1980, pp. 456-461.
[21] Jakirlic, S., Hanjalic, K. & Tropea, C. Modeling rotating and swirling turbulent flows: A perpetual challenge. *AIAA J.* Vol. 40, 2002, pp. 1984–1996.
[22] Versteeg, H. & Malalasekera, W., *An Introduction to Computational Fluid Dynamics*, Pearson Education Limited, 2007.
[23] Kunz, P., Hirschler, M., Huber, M. & Nieken, U., Inflow/outflow with Dirichlet boundary conditions for pressure in ISPH, *Journal of Computational Physics*, Vol.326, 2016, pp. 171-187.
[24] Li, Y., Rowinski, H.D., Bansal, K., & Reddy, R.K., CFD modeling and performance evaluation of a centrifugal fan using a cut-cell method with automatic mesh generation and adaptive mesh refinement, *International Compressor Engineering Conference*, 2018.
[25] Helvoirt, J., *Centrifugal compressor surge: modeling and identification for control*, PhD Thesis, Technische Universiteit Eindhoven, Netherlands, 2007.
[26] Rong, R., Cui, K., Li, Z. & Wu, Z., Numerical study of centrifugal fan with slots in blade surface, *Procedia Engineering*, Vol.126, 2015, pp. 588-591.